Applicability of the Langley Method for Non-Geostationary In-Orbit Satellite Effective Isotropic Radiated Power Estimation

Domenico Cimini, Frank S. Marzano, *Fellow, IEEE*, Marianna Biscarini, *Member, IEEE*, Rebeca Martinez Gil, Peter Schlüssel, Filippo Concaro, Matteo Marchetti, *Graduate Student Member, IEEE*, Marco Pasian, *Senior Member, IEEE*, and Filomena Romano

***Abstract*— The effective isotropic radiated power (EIRP) is a crucial parameter characterizing the transmitting antennas of a radio frequency satellite link. During the satellite commissioning phase, the requirements compliance of communication subsystems is tested. One of the required tests concerns the EIRP of the satellite transmitting antenna. Ground-based power measurements of the satellite-emitted signal are collected to measure EIRP, provided that an estimate of the atmospheric losses is available from independent ancillary measurements or model data. This article demonstrates the applicability of the so-called Langley method to infer EIRP and atmospheric attenuation simultaneously from ground-based power measurements, with no need for ancillary measurements. It is shown that the proposed method gives results similar to more traditional methods, without prior information on atmospheric attenuation. Thus, the proposed method can be applied to monitor EIRP throughout the satellite lifetime from ground-based power measurements alone.**

***Index Terms*— Antenna radiation patterns, radio propagation, satellite antennas.**

I. Introduction

THE effective isotropic radiated power (EIRP) is a parameter characterizing transmitting antennas. EIRP is equal to the product of the transmitted peak power and antenna maximum gain, and thus, it represents one of the driving parameters for the design of a satellite radio frequency (RF) link budget [24]. The driving relation of a satellite link-budget design is the Friis line-of-sight (LOS) equation describing the power received at the end of a point-to-point link as a function of the transmitter/receiver parameters (e.g., spacecraft EIRP and ground antenna gain) as well as atmospheric and free-space losses [14]. Depending on the mission objectives, this equation can be handled in order to design different operational parameters such as the transmitted power or the transmission data rate, provided an accurate knowledge of the atmospheric and free-space losses and transmitter/receiver parameters. Any error in the knowledge of these factors will impact the satellite link-budget design, leading to channel state oversizing (causing data losses) or undersizing (causing a waste of channel resources) (see [12], [13]).

Ground-station antenna specifications are supposed to be stable and easy-to-check, whereas this is not true for the spacecraft components. For any newly launched satellite, the nominal system specifications measured at the ground need to be tested during the commissioning phase, and deviations shall be quantified. In this perspective, the RF in-orbit test (IOT) campaign aims at verifying the requirements compliance of the satellite communication subsystems. One of the required tests concerns the EIRP, one of the most critical quantities characterizing the satellite transmitting sub-system [22]. For nongeostationary satellite, the EIRP assessment during the IOT is even more difficult due to the variable pointing of the ground antenna and the corresponding variable atmospheric loss. During the RF IOT, the EIRP value and stability are monitored by taking ground-based power measurements of the signal emitted by the satellite along its overpasses (see [16], [17]). A procedure to estimate the nongeostationary satellite EIRP is provided by the International Telecommunication Union (ITU) in the recommendation ITU-R S.1512 [23], where the test equipment involves an Earth station, a spectrum analyzer, and a computer for the test program. In this context, to account for atmospheric losses, an estimate of the atmospheric attenuation must be available, either from ancillary measurements or weather model data.

In this work, we propose a method to simultaneously estimate both nongeostationary satellite EIRP and atmospheric

Manuscript received December 20, 2019; revised September 7, 2020; accepted December 6, 2020. This work was designed and supported by the European Organization for the Exploitation of Meteorological Satellites (EUMETSAT) under Grant EUM/CO/18/4600002215/RMG. *(Corresponding author: Domenico Cimini.)*

Domenico Cimini and Filomena Romano are with the National Research Council of Italy, Institute of Methodologies for Environmental Analysis, 85050 Potenza, Italy (e-mail: domenico.cimini@imaa.cnr.it; filomena.romano@imaa.cnr.it).

Frank S. Marzano and Marianna Biscarini are with the Department of Information Engineering, Electronics and Telecommunications (DIET), Sapienza University of Rome, 00184 Rome, Italy, and also with the Center of Excellence CETEMPS, University of L'Aquila, 67100 L'Aquila, Italy (e-mail: frank.marzano@uniroma1.it; marianna.biscarini@uniroma1.it).

Rebeca Martinez Gil and Peter Schlüssel are with the European Organisation for the Exploitation of Meteorological Satellites (EUMETSAT), D-64295 Darmstadt, Germany (e-mail: martinez.gil@eumetsat.int; peter.schluessel@eumetsat.int).

Filippo Concaro is with the European Space Agency (ESA), Darmstadt, Germany (e-mail: filippo.concaro@esa.int).

Matteo Marchetti and Marco Pasian are with the Department of Electrical, Computer and Biomedical Engineering, University of Pavia, 27100 Pavia, Italy (e-mail: matteo.marchetti01@universitadipavia.it, marco.pasian@unipv.it).

Color versions of one or more figures in this article are available at https://doi.org/10.1109/TAP.2020.3048479.

Digital Object Identifier 10.1109/TAP.2020.3048479

attenuation from ground-based power measurements alone by applying the so-called Langley method (LM), with no need for ancillary measurements or weather model data. A historical review of the LM is given in [1]. The LM is named after Samuel Pierpont Langley, the inventor of the bolometer [2], and it involves combining radiation measurements through a range of elevation angles. The traditional LM consists in plotting the radiation intensity (in log scale) versus the airmass factor (a function of elevation angle) and fitting a linear curve to determine the intercept and the slope, which are related to, respectively, the intensity outside the atmosphere and the atmospheric attenuation. The LM can be applied in different contexts of atmospheric sciences, e.g., for the calibration of Sun photometers [3] and microwave radiometers (MWRs) [4], used extensively in operational networks [5]–[7]. One classic application of the LM is the measurement of the Sun irradiance at the top of the atmosphere along with the atmospheric attenuation via ground-based actinometric measurements under varying observation angles [8]. This approach has been more recently extended to the measurement of Sun microwave brightness temperature through Sun-tracking radiometric observations [9], [10].

These latter conditions, i.e., an MWR pointing at the Sun during daytime, are similar to the conditions of an RF link between the ground and a low-Earth-orbit (LEO) satellite (i.e., a receiving antenna pointing at the transmitting satellite during its overpass). Then, the LM can be thought to be applicable for measuring the satellite transmitted power and thus EIRP in the same way, i.e., by angular sampling of ground-based RF received signals during a satellite overpass. To our knowledge, this approach has never been attempted before. This work aims at demonstrating the applicability of the LM to infer EIRP and atmospheric attenuation simultaneously from ground-based power measurements, allowing future satellite missions performing on-flight monitoring of nongeostationary spacecraft EIRP without requiring other external information. In summary, the novelty of the proposed approach with respect to classical LM applications consists in the following:

1) application to a completely different problem, i.e., artificial satellite signals transmission in the microwave domain instead of solar radiation in the visible spectrum;
2) stand-alone on-flight experimental estimation of EIRP with simultaneous estimation of atmospheric attenuation, currently unavailable during the satellite in orbit lifetime;
3) demonstration during typical nongeostationary RF link conditions, including clear and cloudy sky and low-elevation angles, which candidates the proposed method for operational satellite EIRP monitoring during RF-IOT phase and beyond.

This article is organized as follows. Section II develops the theory, Section III presents the available data set, Section IV shows the results, and Section V summarizes the conclusions and outlook.

II. Theoretical Background

The LM follows by applying the Beer–Lambert–Bouguer law to the radiation intensity emitted by an extra-terrestrial source (I_0) and transmitted through the atmosphere along the path forming the zenith angle θ with respect to the surface normal [1]

$$I(\theta) = I_0 \cdot e^{-m(\theta)\tau} \tag{1}$$

where τ is the atmospheric opacity along the zenith direction and $m(\theta)$ is the airmass factor, i.e., a function of zenith angle θ. Frequency dependence in (1) is avoided for simplicity of notation. By taking the natural logarithm, we obtain the classical equation for the LM

$$\ln(I(\theta)) = \ln(I_0) - m(\theta)\tau. \tag{2}$$

In the traditional LM, $\ln(I(\theta))$ is plotted versus $m(\theta)$ and a linear regression performed to determine the intercept $\ln(I_0)$ and the slope $\tau(\nu)$. This approach is often also referred to as Langley extrapolation or Langley plot. Although other formulations of the LM have been proposed, the choice of the traditional LM versus the alternative methods seems more a matter of taste than accuracy (see [11]).

Considering satellite-to-Earth downlink transmissions, EIRP (hereafter indicated with E within equations) is defined as the product of the satellite transmitting antenna maximum gain (G_{SA}) and the total radiated power (P_T)

$$E = G_{SA} P_T. \tag{3}$$

The signal power received by a ground station (P_{GS}) is linked to EIRP through the link budget of an LOS radio communication system

$$P_{GS} = P_T \left(\frac{G_{SA} G_R}{L_T L_R L_{POL}} \right) \frac{1}{L_A L_F} = \left(\frac{E G_R}{L_R L_T L_{POL}} \right) \frac{1}{L_A L_F} \tag{4}$$

where G_{SA} and G_R are the maximum gain of the satellite and ground-station antennas, L_T and L_R are the depointing losses for the transmitting and receiving antenna, L_{POL} is the loss due to polarization mismatch, and L_A and L_F are the atmospheric path loss (due to attenuation by atmospheric gases and hydrometeors) and free-space loss (due to beam divergence), respectively.

For the optimization of the satellite-to-Earth data-transfer, the spacecraft transmission operational parameters are designed through (4) to guarantee a signal-to-noise ratio higher than the minimum threshold required by the receiving system (see [12], [13]). On the other hand, the satellite EIRP can be estimated from (3) by knowing the atmospheric and free-space path losses, the receiver antenna gain, and the measured power at the station. G_R is a parameter of the ground station and L_F is a function of the range d and wavelength λ and can be easily computed by knowing the elevation angle of the receiver ground antenna

$$L_F = \left(\frac{4\pi d}{\lambda} \right)^2. \tag{5}$$

Note that (4) is simply a recasting of the classical Friis equation [14], [15], based on the equivalent dipole antenna model in the case of free-space communications, but considering the impact of Earth's atmosphere through the atmospheric path

loss L_A, which depends on d and the atmospheric optical properties (i.e., the extinction coefficient α) along the link path s

$$L_A = e^{\int_0^d \alpha(s)ds}. \tag{6}$$

The extinction coefficient α depends on atmospheric thermodynamical features, such as pressure, temperature, and humidity, and the presence hydrometeors (cloud and rain droplets). In the assumption of a plane parallel atmosphere, L_A can be expressed in terms of the atmospheric opacity τ at zenith and the airmass factor m

$$\tau = \int_0^{Z_{TOA}} \alpha(z)dz \tag{7}$$

$$m = \frac{1}{cos\theta} = sec\theta \tag{8}$$

$$L_A = e^{m\tau}. \tag{9}$$

The atmospheric path attenuation A(dB) is simply derived from the atmospheric opacity τ(Np) through the multiplicative factor 4.343

$$A(\theta) = 4.343 m(\theta)\tau. \tag{10}$$

A. EIRP Estimation With the Friis Method

The Friis equation (4) may be recasted to obtain EIRP from the other factors, i.e.,

$$E = P_{GS} L_A L_F L_T L_R L_{POL} / G_R. \tag{11}$$

To determine E with (11), hereafter referred to as the Friis method (FM), all the right-hand terms must be known: characteristics of the receiving system (G_R and L_R), measured P_{GS}, link geometry (i.e., L_F), and atmospheric path loss L_A. The critical term is path loss L_A: condition-dependent atmospheric attenuation is required to assess EIRP. Atmospheric attenuation must be estimated from an external source, e.g., applying a propagation model to ancillary measurements, such as radiosonde observations (RAOB) or ground-based MWR observations, or atmospheric simulations, such as 4-D fields from numerical weather prediction (NWP) reanalysis.

B. EIRP Estimation With the LM

The LM can potentially offer a tool to estimate EIRP in alternative to the FM described above. However, it shall be noted that all the applications reviewed in Section I use sources (the Sun or cosmic background) that are very far from the receiving system. As such, the relative distance between the source and the receiver, and thus the free-space loss (5), can be considered constant during the elevation scan. Conversely, when the source is located aboard an LEO satellite, at an altitude of the order of ~1000 km, the relative distance between the transmitting and receiving antennas changes significantly along the overpass. The free-space loss cannot be considered constant, as it changes with zenith angle with the distance

$$L_F(\theta) = \left(\frac{4\pi d(\theta)}{\lambda}\right)^2. \tag{12}$$

In the first approximation, the distance depends on the zenith angle through the height of satellite orbit (h), the Earth radius (R_E), and the elevation angle ($\varphi = (\pi/2) - \theta$) as

$$d(\theta) = \sqrt{(R_E + h)^2 + R_E^2 - 2(R_E + h)R_E sin\alpha} \tag{13}$$

where

$$\alpha = \varphi + sin^{-1}\left[\frac{\cos\varphi}{1 + h/R_E}\right]. \tag{14}$$

Thus, by defining

$$P_1 = EG_R / L_T L_R L_{POL} \tag{15}$$

the EIRP definition (9) can be rewritten as

$$P_{GS}(\theta)L_F(\theta) = P_1 e^{-m(\theta)\tau} \tag{16}$$

and thus

$$\ln(P_{GS}(\theta)L_F(\theta)) = \ln(P_1) - m(\theta)\tau \tag{17}$$

which is suitable to be treated using the LM. Considering a transmitting antenna on an LEO satellite, ground-based measurements of P_{GS} at different elevation angles, i.e., different values of the airmass $m(\theta)$, may be collected by tracking the satellite during each overpass. Thus, measurements in the $(\ln(P_{GS}(\theta)L_F(\theta)),\ m(\theta))$ plane can be fitted by a straight line. The slope and the intercept to zero airmass of the line fit correspond to the atmospheric opacity τ and $\ln(P_1)$, respectively. Once $\ln(P_1)$ is determined, P_1 may be derived and, thus, EIRP, assuming that L_T, L_R, L_{POL}, and G_R are known

$$E = \frac{P_1}{G_R} L_T L_R L_{POL}. \tag{18}$$

III. Data Set

The data set collected in this study for demonstrating the applicability of the LM for EIRP measurements includes both ground-based observations and model data from global reanalysis.

A. RF Link Measurements

The primary data set consists in ground-based power measurements of RF signals emitted by a *Ka*-band downlink aboard an LEO satellite. These measurements are collected in the framework of a European Space Agency (ESA) project named Svalbard grouNd statiOn for Wide Band Earth observation data Reception (SNOWBEAR) [16], [17]. The receiving antenna, protected by a radome, is located on the Platåberge plateau (78.2272392 °N, 15.4339544 °E, 499.5 m a.s.l.), within the Svalbard Satellite Station (SVALSAT), ~2 km from the Svalbard airport near Longyearbyen, Norway. SNOWBEAR takes place within the EUMETSAT Polar System–Second Generation (EPS-SG) mission to derisk the introduction of the 26 GHz transmission band [18]. The LEO satellite is the Joint Polar Satellite System 1 (JPSS-1, called NOAA-20 after commissioning). JPSS-1 is equipped with a *Ka*-band downlink that shares a lot of commonalities with the one that will be mounted on MetOP-SG, the core

TABLE I
CHARACTERISTICS OF RECEIVING SYSTEM

Frequency band	25.5 – 27.0 GHz
Operational frequency	26.7034 ± 0.150 GHz
Polarization	RHC & LHC simultaneously
3dB beamwidth	0.1°
Antenna gain	64.17 dB

spacecraft of EPS-SG mission. The JPSS-1 Radio Frequency Interface Control Document (see [19]) reports a 45.0 dBW nominal value for EIRP, estimating the operational value to be 43.51 dBW by accounting for antenna gain and other system losses. The main characteristics of the *Ka*-band receiving system are shown in Table I.

NOAA-20 orbit has a repetition cycle of 227 passes (16 days, 14/15 passes per day), of which 205 are with maximum elevation $<80°$, whereas the remaining 22 have maximum elevation $>80°$. Ground-based measurements during 73 passes from December 2018 to May 2019 have been considered in this study, including low-, medium-, and high-elevation pass-type conditions. Measurements at the RHCP channel (cryogenic chain) are considered, particularly the broadband RF Signal power at the high data rate receiver input (HRD2). Fig. 1 shows one example of data for a high-elevation orbit overpass.

B. Model Data

The model data identified for this study are the global reanalysis available from the European Center for Medium-range Weather Forecast (ECMWF). The current generation of ECMWF atmospheric reanalysis (ERA5) provides hourly data of many atmospheric, land-surface, and sea-state parameters. ERA5 data are available from the Copernicus Climate Change Service (C3S) Climate Data Store (CDS). Monthly updates of the ERA5 data set are currently published within three months from real time. Atmospheric fields are defined on regular latitude–longitude grid and 37 vertical levels up to 0.01 hPa. The spatial resolution is $0.25° \times 0.25°$, corresponding to roughly 27.8×5.7 km at Svalbard latitudes. The closest ECMWF global reanalysis grid point is about 3 km far from the SNOWBEAR site. ERA5 data closest to the dates/times of the 73 overpasses have been obtained from the C3S-CDS.

Atmospheric attenuation depends on the atmospheric thermodynamical conditions. In particular, the absorption of each atmospheric layer depends on temperature, pressure, and water (vapor and liquid) content. Atmospheric attenuation at any frequency and observing angle can be computed by processing the closest the ERA5 thermodynamical profiles with a radiative transfer (or atmospheric propagation) model. As such, a modeled estimate of atmospheric attenuation can be produced for any grid point within 1 h from each satellite overpass by processing ERA5 atmospheric profiles. The accuracy of such estimate depends on the uncertainty of the ERA5 profiles in representing the real atmospheric conditions, as well as the uncertainty of the absorption model.

Fig. 2 shows the integrated water vapor (IWV) and liquid water path (LWP), obtained integrating ERA5 specific

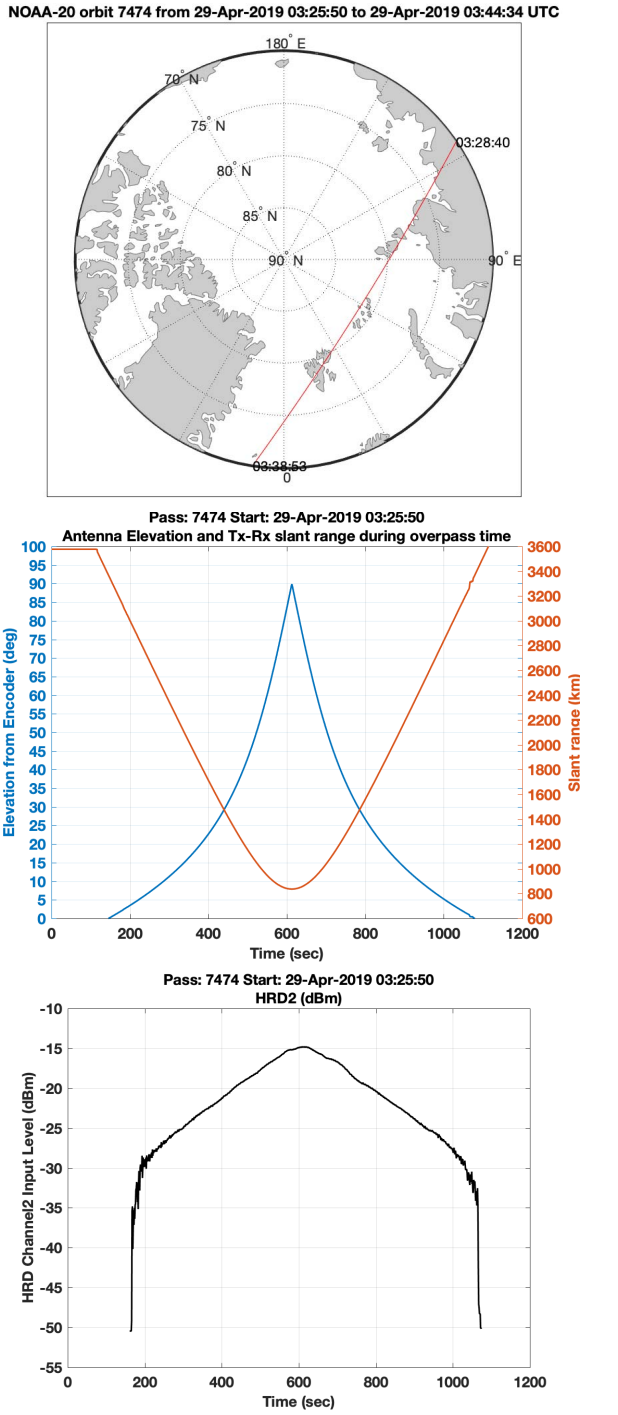

Fig. 1. Example of RF link measurements during a high-elevation pass (#7474 on April 29, 2019 from 03:25 to 03:44 UTC). Top: NOAA-20 satellite orbit track. Middle: antenna elevation (blue) and transmitter–receiver slant range (red) versus recording time. Bottom: HRD2 channel input level versus recording time.

humidity and liquid water content profiles, as well as the attenuation maps obtained for each ERA5 grid point. The attenuation is computed at 500 m a.s.l. to simulate the conditions at the SNOWBEAR site.

IV. RESULTS

The RF link data described in Section III are used to estimate the value of EIRP with both the FM and the LM.

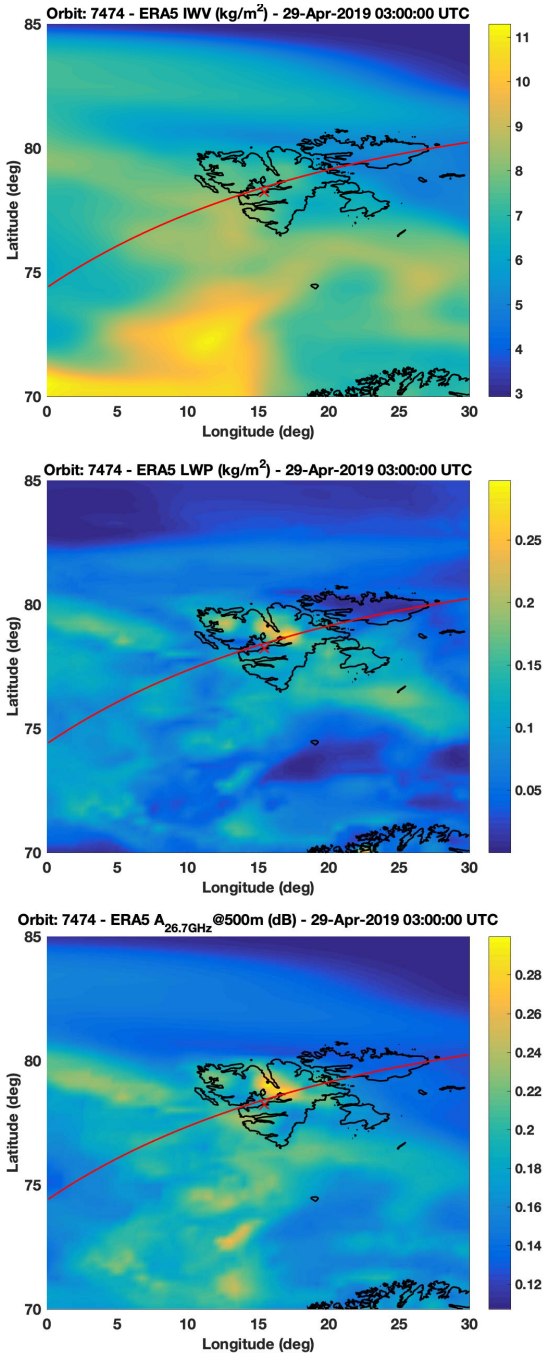

Fig. 2. IWV (top) and LWP (middle) obtained integrating specific humidity and liquid water content profiles for each ERA5 grid point. Corresponding total attenuation (bottom) computed at 500 m a.s.l. to simulate atmospheric attenuation at the SNOWBEAR site. ERA5 date/time is the closest to the satellite pass in Fig. 1.

The simulated attenuation computed as above is used as the ancillary information needed by the FM, while it represents an independent source of comparison for the attenuation inferred by the LM.

Note that the original formulations, i.e., (11) for the FM and (17) and (18) for the LM, have been modified to dB units, respectively, as follows:

$$E_{FM} = P_{GS} + L_A + L_F + L_T + L_R + L_{POL} - G_R \quad (19)$$

$$P_{GS} + L_F = P_1 - mL_A \quad (20)$$

$$E_{LM} = P_1 + L_T + L_R + L_{POL} - G_R. \quad (21)$$

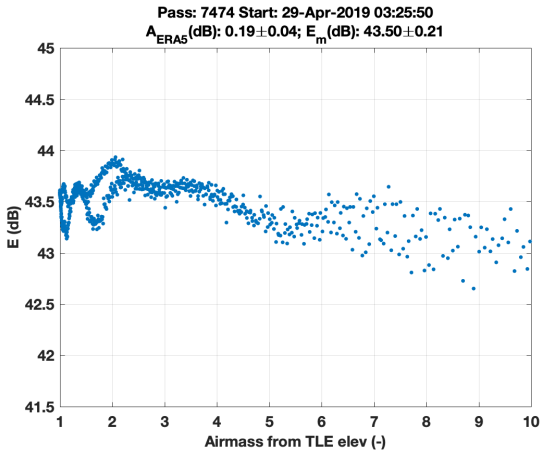

Fig. 3. EIRP estimated with the FM for the overpass in Fig. 1 (#7474, April 29, 2019, started 03:25 UTC). The attenuation from ERA5 and the EIRP mean value ± one std are reported above the panel.

Values in the equations above are obtained from the following sources.

1) P_{GS}: Ground-based measurements of received power at different antenna elevation angles. Measurements at the HRD2 channel are used. P_{GS} is estimated from the HRD2 receiver signal accounting for all the losses within the cryogenic chain, as provided by the SNOWBEAR signal-level plan. Antenna elevation angles are encoded within the file, from which the zenith angles θ are derived.
2) L_A: For the FM, the atmospheric path loss is calculated from the simulated atmospheric opacity computed from ERA5 profiles on the grid point closest to the SNOWBEAR site, computed at 500 m a.s.l. For the LM, L_A is estimated together with P_1, as the linear fit coefficients (slope and offset, respectively), with no need for ancillary input data.
3) L_F: The free-space loss is calculated from the distance between the orbiting transmitter and the ground-based receiver, which is encoded within the overpass data files.
4) L_R, L_T, *and* L_{POL}: The losses for the transmitting and receiving systems, as well as the polarization losses are provided by ESA/EUMETSAT for the SNOWBEAR antenna or from analogy with other missions.
5) G_R: The gain of the ground-station antenna is provided by the SNOWBEAR signal level plan (see Table I).

One example of FM results obtained applying (19) to one RF link data file is shown in Fig. 3. As implicit in the FM, once L_A is provided, each measurement P_{GS} at any given pointing angle provides one estimate of EIRP. In the example in Fig. 3, L_A from ERA5 is 0.19 dB, resulting in EIRP estimates ranging from 42.6 to 43.9 dB. The mean value E_{FM} is 43.50 ± 0.21 dB where the uncertainty is calculated as 1 std of all the estimates at different angles. The uncertainty associated with single estimate at each angle may also be considered applying a weighted average, though it does not change the results significantly (in this case 43.51 ± 0.21 dB).

The results for the LM obtained applying (20) and (21) to the same overpass are shown in Fig. 4. The retrieved values for E_{LM} and L_A are, respectively, 43.65 ± 0.01 and

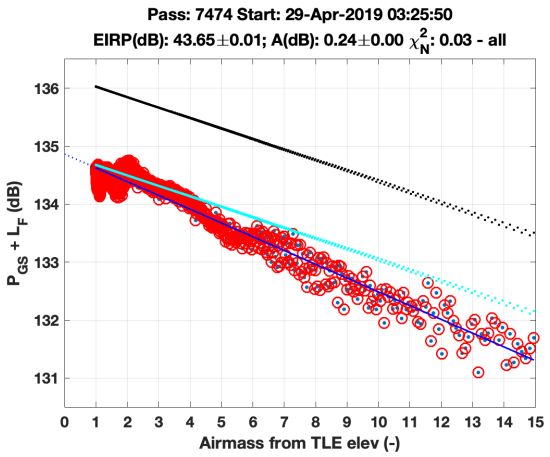

Fig. 4. LM applied to RF link data from the overpass in Fig. 1 (#7474, April 29, 2019, started 03:25 UTC). Blue dots indicate the measured data, whereas red circles highlight the data considered in the linear fit (in this case all between 1 and 15 airmass). The blue solid line indicates the linear fit, extrapolated to zero airmass (dashed line). L_A and P_1 are derived from the linear fit coefficients (slope and intercept, respectively). Then, E_{LM} (dB) is inferred from P_1. The value of the normalized χ^2_N for the linear fit is also shown. Black and cyan dots indicate simulations from ECMWF reanalysis considering, respectively, the EIRP nominal value (45.00 dB) and the EIRP value retrieved with the LM (43.65 dB).

0.24 ± 0.00 dB, where the uncertainties account for the uncertainty of the linear fit coefficients through noisy data, given by the weighted linear regression theory (see [20]). The goodness of the linear fits is quantified through the normalized χ^2_N. To select trustful linear fits, retrievals for which χ^2_N is larger than a threshold, arbitrarily set to 0.1, are discarded.

Note that (20) can be easily modeled knowing hardware specifications (including EIRP) and atmospheric attenuation. Fig. 4 also shows the modeled data using atmospheric attenuation computed from ECMWF reanalysis and assuming two different values for EIRP, the nominal (45.0 dB) and the retrieved value (43.65 dB). Measured and modeled slopes (i.e., atmospheric attenuation) are slightly different, as ECMWF reanalysis map into 0.18 dB, while measurements call for 0.24 dB. Also, the measurements show a wider spread for atmospheric attenuation.

Ideally, the coefficients estimated with the linear fit should not depend significantly on the choice of input data points, as long as the data points express the same linear dependence with some additional random uncertainty. However, undesired spurious effects may cause the data points to depart from the expected behavior. During this analysis, at least four features were found that may hamper the meaningful applicability of the LM.

1) *Depointing Due to Antenna Step-Like Motion:* A sharp drop of the signal when the overpass is reaching its maximum elevation. This is likely due to depointing associated with slow step-like motion of elevation motor. As such, it does not happen at any particular elevation angle, it happens when the elevation angle speed gets close to zero, i.e., when the elevation angle gets close to the maximum value of that pass.
2) *Snow Accumulation Over the Radome:* During winter, snow may accumulate over the antenna radome, despite the regular cleaning. Snow accumulates especially on the top, causing additional attenuation at high elevation angles, but shows uneven distribution due to local conditions of insulation, wind speed, and direction.
3) *High Pass Depointing During Descending:* For passes reaching 80° elevation, the antenna is moved by a combination of cross-elevation and elevation motors. For these passes, there seems to be a systematic depointing during the descending phase. This may suggest that the alignment between autotrack and antenna axes may be optimized for the range 0°–90° but not for 90°–180° when the antenna feed is upside-down. This feature would cause additional depointing and thus a drop in the signal, as seen in spring/summer months, when the snow accumulation is to be excluded.
4) *Near-Field Obstructions:* A metal gear (∼30 cm × 50 cm) is located on top of the radome, which serves for holding a lamp and for rotating the rope for snow removal. It is likely that the metal gear causes signal disturbance when seen by the principal reflector, though the geometry is difficult to characterize as the gear sits within the antenna near field.

For the reasons above, it is clear that the selection of data points may be important for the linear fit. Therefore, we identified a range of airmass in which the above features did not show evidently (from 3 to 10 airmass, i.e., from ∼20° to 5° elevation, ascending only) to apply the LM. The rest of this section considers only LM applied to this data set, if not otherwise specified.

The results of the LM for the available overpasses are compared with other sources of EIRP and atmospheric attenuation. In particular, EIRP and atmospheric attenuation from LM are compared, respectively, with EIRP computed with the FM and atmospheric attenuation calculated from ERA5 profiles. Fig. 5 shows the comparison of E_{LM} versus E_{FM}. The two methods agree within 0.46 dB root mean square (rms), with a relatively small bias (0.14 dB) and fairly high correlation (0.8). The mean values of EIRP as estimated with FM and LM are 44.19 (0.63) and 44.25 (0.86) dB, respectively (values in parenthesis are 1 std).

Finally, Fig. 6 shows the comparison of atmospheric attenuation retrieved with the LM and computed from ERA5 profiles. The two methods agree within 0.09 dB rms, with a relatively small bias (0.01 dB) and medium correlation (0.7).

Note that the results above are obtained regardless of atmospheric conditions (clear and cloudy), despite the fact that the LM implies homogenous atmospheric attenuation during observations at different elevation angles. This is a fair approximation in clear and stable sky conditions, while it may become weak in the presence of dynamical weather, e.g., front passage, convection, and broken clouds. One possible mitigation is cloud screening, i.e., an automated process that identifies and removes points that are judged not consistent with clear sky conditions. A cloud screening developed for LM applied to direct-beam solar radiation is proposed in [21]. The method is equivalent to the LM but with an additional iterative screening before fitting the data. It was shown capable of detecting direct-beam solar radiation observations in short

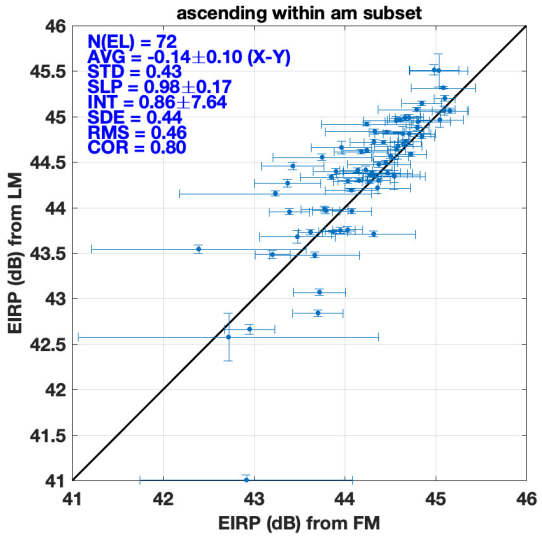

Fig. 5. Scatter plot of E_{LM} versus E_{FM}. The table reports sample size [N(EL)], average (AVG), standard deviation (STD), and rms of the X − Y difference, slope (SLP), intercept (INT), and estimated statistical error (SDE) of the linear fit, and correlation coefficient (COR) between X and Y. Values after ± indicate 95% confidence interval. Units for AVG, STD, INT, SDE, and rms are dB.

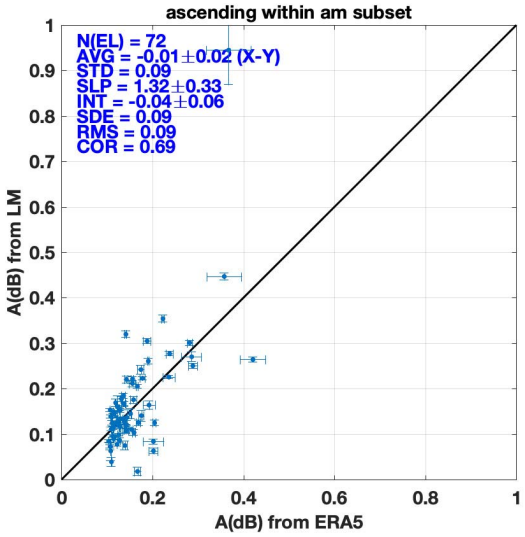

Fig. 6. Scatter plot of A_{LM} versus A_{ERA5}. The table reports sample size [N(EL)], average (AVG), standard deviation (STD), and rms of the X − Y difference, slope (SLP), intercept (INT), and estimated statistical error (SDE) of the linear fit, and correlation coefficient (COR) between X and Y. Values after ± indicate 95% confidence interval. Units for AVG, STD, INT, SDE, and rms are dB.

clear windows. However, conditions differ here, especially because antenna beam and cloud contamination are, respectively, larger and weaker at *Ka*-band relative to solar radiation. When applied to the available data set, this screening did not appear to improve the results, despite an increased processing time due to the iterative approach. Despite the rather neutral impact, we recognize that data screening is an important aspect that is worth further investigation; however, with the present data set, the abovementioned issues are far more impacting than atmospheric inhomogeneity.

V. Conclusion

This study demonstrates the applicability of the LM for measurements of satellite antenna EIRP. The results from the LM have been compared against the traditional FM.

A reduced range of elevation angles has been identified (5°–20°) to mitigate the impact of the undesired features affecting the available data set, i.e., depointing due to antenna step-like motion, snow accumulation over the radome, depointing during descending, and near-field obstructions. From the available data set and the period under analysis, the primary results are as follows.

1) EIRP retrieved with the LM agrees with FM with mean square (rms difference < 0.46 dB, bias < 0.14 dB, and correlation $= 0.8$).
2) Atmospheric attenuation retrieved with the LM agrees with ERA5 simulations with rms difference < 0.09 dB, bias < 0.01 dB, and correlation $= 0.7$.

The results above indicate that the LM is indeed applicable for the simultaneous and self-consistent estimate of atmospheric attenuation and EIRP of the satellite antenna. With respect to the more conventional FM, the LM only requires angular sampling of ground-based power measurements of RF signals with no need for ancillary measurements or weather model data. In this sense, the LM can be referred to as a self-consistent approach to satellite EIRP estimation.

This study paves the way to the ground-based self-consistent estimate of satellite EIRP, which can be applied to several nongeostationary currently orbiting satellites as well as to future satellites, e.g., MetOP-SG series of the EUMETSAT EPS-SG mission. However, there remain a few issues so that the proposed approach would benefit from further investigation of the following aspects:

1) impact of atmospheric inhomogeneity on EIRP estimation and feasibility of adaptive data screening;
2) larger range of atmospheric attenuation, currently limited to conditions typical of Arctic winter and spring;
3) validation with independent sources of atmospheric attenuation, such as available from an MWR colocated with the ground antenna and scanning in satellite-tracking mode;
4) exploration of radio-meteorological forecast based on high-resolution NWP.

Acknowledgment

The authors thank Vinia Mattioli and Tim Hewison, European Organisation for the Exploitation of Meteorological Satellites (EUMETSAT), for the fruitful discussions throughout the study and Salvatore Larosa, National Research Council of Italy, Institute of Methodologies for Environmental Analysis (CNR-IMAA), for helping with satellite orbit information. This work is based on a EUMETSAT idea.

References

[1] G. E. Shaw, "Sun photometry," *Bull. Amer. Meteorol. Soc.*, vol. 64, no. 1, pp. 4–10, 1983, doi: 10.1175/1520-0477(1983)064<0004:SP>2.0.CO;2.
[2] S. P. Langley, "The bolometer and radiant energy," *Proc. Amer. Acad. Arts Sci.*, vol. 16, pp. 342–358, Jun. 1881, doi: 10.2307/25138616.

[3] G. E. Shaw, J. A. Reagan, and B. M. Herman, "Investigations of atmospheric extinction using direct solar radiation measurements made with a multiple wavelength radiometer," *J. Appl. Meteorol. Climatol.*, vol. 12, no. 2, pp. 374–380, 1973, doi: 10.1175/1520-0450(1973)012<0374:IOAEUD>2.0.CO;2.

[4] Y. Han and E. R. Westwater, "Analysis and improvement of tipping calibration for ground-based microwave radiometers," *IEEE Trans. Geosci. Remote Sens.*, vol. 38, no. 3, pp. 1260–1276, May 2000.

[5] B. N. Holben *et al.*, "AERONET—A federated instrument network and data archive for aerosol characterization," *Remote Sens. Environ.*, vol. 66, no. 1, pp. 1–16, Oct. 1998, doi: 10.1016/S0034-4257(98)00031-5.

[6] M. Campanelli, V. Estellés, C. Tomasi, T. Nakajima, V. Malvestuto, and J. A. Martínez-Lozano, "Application of the SKYRAD improved Langley plot method for the *in situ* calibration of CIMEL sun-sky photometers," *Appl. Opt.*, vol. 46, no. 14, p. 2688, May 2007.

[7] M. P. Cadeddu, J. C. Liljegren, and D. D. Turner, "The atmospheric radiation measurement (ARM) program network of microwave radiometers: Instrumentation, data, and retrievals," *Atmos. Meas. Techn.*, vol. 6, no. 9, pp. 2359–2372, Sep. 2013, doi: 10.5194/amt-6-2359-2013.

[8] G. E. Shaw, "Solar spectral irradiance and atmospheric transmission at Mauna Loa observatory," *Appl. Opt.*, vol. 21, no. 11, pp. 2007–2011, 1982, doi: 10.1364/AO.21.002006.

[9] F. S. Marzano, V. Mattioli, L. Milani, K. M. Magde, and G. A. Brost, "Sun-tracking microwave radiometry: All-weather estimation of atmospheric path attenuation at Ka-, V-, and W-band," *IEEE Trans. Antennas Propag.*, vol. 64, no. 11, pp. 4815–4827, Nov. 2016, doi: 10.1109/TAP.2016.2606568.

[10] V. Mattioli, L. Milani, K. M. Magde, G. A. Brost, and F. S. Marzano, "Retrieval of sun brightness temperature and precipitating cloud extinction using ground-based sun-tracking microwave radiometry," *IEEE J. Sel. Topics Appl. Earth Observ. Remote Sens.*, vol. 10, no. 7, pp. 3134–3147, Jul. 2017, doi: 10.1109/JSTARS.2016.2633439.

[11] S. M. Adler-Golden and J. R. Slusser, "Comparison of plotting methods for solar radiometer calibration," *J. Atmos. Ocean. Technol.*, vol. 24, no. 5, pp. 935–938, May 2007.

[12] M. Biscarini *et al.*, "Optimizing data volume return for Ka-band deep space links exploiting short-term radiometeorological model forecast," *IEEE Trans. Antennas Propag.*, vol. 64, no. 1, pp. 235–250, Jan. 2016, doi: 10.1109/TAP.2015.2500910.

[13] M. Biscarini, M. Montopoli, and F. S. Marzano, "Evaluation of high-frequency channels for deep-space data transmission using radiometeorological model forecast," *IEEE Trans. Antennas Propag.*, vol. 65, no. 3, pp. 1311–1320, Mar. 2017, doi: 10.1109/TAP.2017.2653420.

[14] H. T. Friis, "A note on a simple transmission formula," *Proc. IRE Waves Electrons*, vol. 34, no. 5, pp. 254–256, May 1946.

[15] J. A. Shaw, "Radiometry and the Friis transmission equation," *Amer. J. Phys.*, vol. 81, no. 1, pp. 33–37, Jan. 2013, doi: 10.1119/1.4755780.

[16] F. Concaro, M. Marchetti, and M. Pasian, "Preliminary analysis of the performance metrics for the 26 GHz band receiving channel of the SNOWBEAR project," in *Proc. 8th Int. Workshop Tracking, Telemetry Command Syst. Space (TTC)*. Darmstadt, Germany: ESA-ESOC, Sep. 2019, pp. 1–7.

[17] M. Marchetti, D. Lospalluto, F. Concaro, F. Romano, D. Cimini, and M. Pasian, "Performance trends at 26 GHz for a receiving ground station at polar latitudes: The SNOWBEAR project," in *Proc. 14th Eur. Conf. Antennas Propag. (EuCAP)*, Copenhagen, Denmark, Mar. 2020, pp. 1–5.

[18] A. Martellosio *et al.*, "High frequency radomes for ground stations in polar regions: Review of the state of the art and novel developments," *IEEE Antennas Propag. Mag.*, vol. 59, no. 6, pp. 88–101, Dec. 2017.

[19] *Joint Polar Satellite System 1 (JPSS-1) Spacecraft Stored Mission Data (SMD) to Ground Segment (GS) Radio Frequency (RF) Interface Control Document (ICD), Joint Polar Satellite System (JPSS) Program Code 470*, document 470-REF-00171, Jan. 28, 2015.

[20] P. R. Bevington and D. K. Robinson, *Data Reduction and Error Analysis for the Physical Sciences*, 3rd ed. New York, NY, USA: McGraw-Hill, 2003.

[21] M. Chen, J. Davis, and W. Gao, "A new cloud screening algorithm for ground-based direct-beam solar radiation," *J. Atmos. Ocean. Technol.*, vol. 31, no. 12, pp. 2591–2605, 2014, doi: 10.1175/JTECH-D-14-00095.1.

[22] B.-J. Ku, D.-S. Ahn, D.-C. Baek, K.-R. Park, and S.-P. Lee, "Degradation analysis of user terminal EIRP and G/T due to station-keeping variation of stratospheric platform," *ETRI J.*, vol. 22, no. 1, pp. 12–19, Mar. 2000, doi: 10.4218/etrij.00.0100.0102.

[23] *Measurement Procedure for Determining Non-Geostationary Satellite Orbit Satellite Equivalent Isotropically Radiated Power and Antenna Discrimination*, document ITU-R S.1512-0, International Telecommunication Union Document, Sep. 2020, Art. no. E19302. [Online]. Available: https://www.itu.int/dms_pubrec/itu-r/rec/s/R-REC-S.1512-0-200102-I!!PDF-E.pdf

[24] G. Maral and M. Z. B. Sun, Eds., *Satellite Communications Systems: Systems, Techniques and Technology*, 5th ed. Chichester, U.K.: Wiley, 2009. [Online]. Available: https://www.wiley.com/en-it/Satellite+Communications+Systems%3A+Systems%2C+Techniques+and+Technology%2C+6th+Edition-p-9781119382089

Domenico Cimini received the Laurea (*cum laude*) and Ph.D. degrees in physics from the University of L'Aquila, L'Aquila, Italy, in 1998 and 2002, respectively.

Since 2002, he has been a Researcher with the Center of Excellence for Remote Sensing and Modeling of Severe Weather (CETEMPS); a Research Assistant with the Cooperative Institute for Research in Environmental Sciences (CIRES), University of Colorado at Boulder, Boulder, CA, USA; and an Adjunct Professor with the Department of Electrical and Computer Engineering, University of Colorado at Boulder. He is currently a Senior Researcher with the National Research Council of Italy, Institute of Methodologies for the Environmental Monitoring (CNR-IMAA), Potenza, Italy. He has more than 20 years of experience with ground- and satellite-based passive remote sensing, particularly microwave radiometry. He led and participated in several international projects funded by the European Organization for the Exploitation of Meteorological Satellites (EUMETSAT), Darmstadt, Germany, the European Space Agency, and the U.S. Atmospheric Radiation Measurement (ARM) program.

Dr. Cimini is a Life Member of the European Geophysical Union (EGU). He was a recipient of the Fondazione Ugo Bordoni Award in 2008 in memory of Prof. Giovanni D'Auria and the 6th Hans Liebe Lectureship bestowed by the U.S. National Committee (USNC) for the Union of Radio Scientists Internationale (URSI) in 2019.

Frank S. Marzano (Fellow, IEEE) received the Laurea degree (*cum laude*) in electrical engineering and the Ph.D. degree in applied electromagnetics from the Sapienza University of Rome, Rome, Italy, in 1988 and 1993, respectively.

After being a Lecturer with the University of Perugia, Perugia, Italy, in 1997, he joined the Department of Electrical Engineering, University of L'Aquila, L'Aquila, Italy, teaching courses on electromagnetic fields as an Assistant Professor. In 2002, he earned an Associate Professorship and co-founded the Center of Excellence for Remote Sensing and Modeling of Severe Weather (CETEMPS). In 2005, he finally joined the Department of Information Engineering, Electronics and Telecommunications, Sapienza University of Rome, where he teaches courses on antennas, propagation, and remote sensing. Since 2007, he has been the Vice-Director of CETEMPS, University of L'Aquila, where he was nominated as the Director in March 2013. His research interests include passive and active remote sensing of the atmosphere from ground-based, airborne, and space-borne platforms, and electromagnetic propagation studies. He has published more than 140 articles on refereed international journals, more than 30 contributions to international book chapters, and more than 300 extended abstracts on international and national congress proceedings.

Dr. Marzano has been a fellow of the Royal Meteorological Society (RMetS) since 2012. Since January 2011, he has been an Associate Editor of *Atmospheric Measurements Techniques* (EGU). He has been an Associate Editor of the IEEE TRANSACTIONS ON GEOSCIENCE AND REMOTE SENSING since 2014.

Marianna Biscarini (Member, IEEE) received the M.Sc. degree (*cum laude*) in electronic engineering and the Ph.D. degree in electromagnetism from the Sapienza University of Rome, Rome, Italy, in 2012 and 2016, respectively.

Since 2012, she has been with the Department of Information Engineering, Electronics and Telecommunications (DIET), Sapienza University of Rome, and the Center of Excellence for Remote Sensing and Modeling of Severe Weather (CETEMPS), University of L'Aquila, L'Aquila, Italy, working on radiopropagation, numerical modeling and microwave radiometry. She is currently a Research Assistant with DIET. She is involved in several projects in collaboration with the European Space Agency (ESA) and AFRL. Her current research interests include microwave radio propagation, atmospheric modeling, microwave radiometry, and deep-space satellite communications.

Rebeca Martinez Gil received the M.S. degree in electronics and telecommunications engineering from the University of Valencia, Valencia, Spain, in 2003, and the Cork Institute of Technology, Cork, Ireland.

She worked with the European Space Agency, European Space Operation Centre (ESA/ESOC), Darmstadt, Germany. She joined the Exploitation of Meteorological Satellites (EUMETSAT), Darmstadt, in 2009, as a Data Handling and System Engineer for LEO satellites. She is currently working for the EPS-SG mission in the area of space to ground interfaces.

Ms. Martinez Gil received the First National Prize from the Spanish Ministry of Education and Science for her academic achievements in 2004.

Peter Schlüssel received the Diploma degree in meteorology and the Dr.rer.nat. degree from the Universität Kiel, Kiel, Germany, in 1983 and 1987, respectively, and the Dr.habil. degree in meteorology from the Universität Hamburg, Hamburg, Germany, in 1995.

He is currently a Staff Member with the European Organisation for the Exploitation of Meteorological Satellites (EUMETSAT), Darmstadt, Germany, where he serves as an EPS-SG Program Scientist.

Filippo Concaro graduated in electronic engineering from the University of Pavia, Pavia, Italy, in 2003, after a six-month traineeship at the Ground Station Antenna (GSA) Section, European Space Operation Centre (ESOC), Darmstadt, Germany.

Since 2013, has been always working in ESOC, despite a parenthesis of one year at the European Organisation for the Exploitation of Meteorological Satellites (EUMETSAT), Darmstadt. He was involved in the design and testing of several Ground station projects all over the European Space Agency Tracking Network (ESTRACK). In particular, he was a Technical Officer of several projects as the three XAA (X-Band Acquisition Aid) terminals in Perth, Australia; Kourou (French Guyana), and Maspalomas (Canary Islands) and the NNO-2 in New Norcia, WA, Australia, and MAL-X in Malindi, Kenia, antennas, which provided ESA with the capacity to support complicated Launch and Early Orbit Phase (LEOP) operations for X-Band satellites. He is responsible for the SNOWBEAR Project, a 6.4 m antenna terminal for High Data Rate reception at Svalbard, Norway, and also involved in several other ESA developments ranging from large deep space antennas (up to 64 m diameter) to small acquisition terminals (down to 0.7 m) and from theoretical studies to operational applications.

Matteo Marchetti (Graduate Student Member, IEEE) was born in 1992. He received the M.Sc. degree in electronic engineering from the University of Pavia, Pavia, Italy, in 2018, where he is currently pursuing the Ph.D. degree with the Microwave Laboratory.

He joined the European Space Agency, Darmstadt, Germany, in 2018. His research interests are in the fields of microwave and millimeter-wave components and technologies for space applications. In particular, satellite-to-ground station communication links, radomes, reflector antennas, and dichroic mirror designs.

Marco Pasian (Senior Member, IEEE) was born in 1980. He received the M.Sc. degree (*cum laude*) in electronic engineering and the Ph.D. degree in electronics and computer science from the University of Pavia, Pavia, Italy, in 2005 and 2009, respectively.

He held a post-doctoral position at the University of Pavia from 2009 to 2013. He joined the European Space Agency, Darmstadt, Germany, in 2004; Carlo Gavazzi Space, Milan, Italy, in 2005; and the TNO, Defense, Security and Safety, Rijswijk, The Netherlands, in 2008. Since 2013, he has been a Research Fellow/an Assistant Professor with the Microwave Laboratory, University of Pavia, where he has been an Associate Professor since 2020. His research interests are in the fields of microwave and millimeter-wave components and technologies for space applications, in the fields of biomedical applications, substrate integrated waveguide, and microwave-based snow monitoring. He is the Principal Investigator (PI) of the Italian SIR2014 project "SNOWAVE" and the European Union INTERACT TA projects "ARCTICWAVE" (2019) and "ARCTIC-GBR" for the term 2020–2021, all on snowpack monitoring. He was the PI of a grant funded by the University of Pavia under the call INROAd and the Unit Leader for the Italian PRIN2017 project "WPT4WID," both on biomedical applications. He is also the Project Manager, the Scientific Manager, or a Consultant for several projects in collaborations with Italian and European research centers and/or industries, including the European Space Agency.

Dr. Pasian is a member of the European Microwave Association (EuMA) and the Italian Society on Electromagnetism (SIEm). He was the Technical Program Co-Chair of the European Microwave Conference in 2014 and the Conference Prize Committee Chair at European Microwave Week in 2014 and the Finance Chair of the IEEE International Conference on Numerical and Electromagnetic Modeling and Optimization and the IEEE MTT-S International Microwave Workshop Series-Advanced Materials and Processes. He is also an Associate Editor of the IEEE JOURNAL OF ELECTROMAGNETICS, RF AND MICROWAVES IN MEDICINE AND BIOLOGY and the *EuMA International Journal of Microwave and Wireless Technologies*.

Filomena Romano received the M.S. degree in physics from the University of Bologna, Bologna, Italy, in 1990.

In 1992, she joined the Institute of Methodologies for Environmental Analysis, Tito Scalo, Italy, where she got experience on experimental and theoretical studies in atmospheric remote sensing. She collaborated in studies concerning retrieval of atmospheric aerosol from solar spectra at ground level. She has currently specialized in satellite data handling for meteorological and climatological studies. Her main research interests include cloud detection, cloud clearing, and cloud microphysical retrieval of infrared and microwave radiance from spaceborne sensors are her main activities.